European Polymer Journal 49 (2013) 991–998

Contents lists available at SciVerse ScienceDirect

European Polymer Journal

journal homepage: www.elsevier.com/locate/europolj

Macromolecular Nanotechnology

Characterization of polyaniline–detonation nanodiamond nanocomposite fibers by atomic force microscopy based techniques

D. Passeri [a,*], A. Biagioni [a], M. Rossi [a,c], E. Tamburri [b], M.L. Terranova [b]

[a] Department of Basic and Applied Sciences for Engineering, University of Rome Sapienza, Via A. Scarpa 16, 00161 Rome, Italy
[b] Department of Chemical Sciences and Technologies, University of Rome Tor Vergata and Micro and Nano-structured Systems Laboratory (MINASlab), Via della Ricerca Scientifica, 00133 Rome, Italy
[c] Centro di Ricerca per le Nanotecnologie Applicate all'Ingegneria della Sapienza (CNIS), University of Rome Sapienza, Piazzale A. Moro 5, 00185 Rome, Italy

ARTICLE INFO

Article history:
Received 16 August 2012
Received in revised form 28 January 2013
Accepted 3 February 2013
Available online 13 February 2013

Keywords:
Atomic force microscopy
Polyaniline fibers
Nanodiamond
Mechanical properties
Electrical properties

ABSTRACT

Polyaniline (PANI) fibers were synthesized in presence of detonantion nanodiamond (DND) particles by precipitation polymerization technique. Morphological, electrical and mechanical characterizations of the obtained PANI/DND nanocomposited have been performed by different either standard or advanced atomic force microscopy (AFM) based techniques. Morphological characterization by tapping mode AFM supplied information about the structure of fibers and ribbons forming the PANI/DND network. An AFM based technique that takes advantage of an experimental configuration specifically devised for the purpose was used to assess the electrical properties of the fibers, in particular to verify their conductivity. Finally, mechanical characterization was carried out synergically using two different and recently proposed AFM based techniques, one based on AFM tapping mode and the other requiring AFM contact mode, which probed the nanocomposited nature of PANI/DND fiber sample down to different depths.

1. Introduction

Polymeric micro- and nano-fibers, nanorods and nanotubes have been proposed for a wide number of applications, e.g., humidity, temperature and gas sensing [1,2], drug release [3], or electroactive actuators [4–6]. To improve the performances of the devices, polymers filled with nanomaterials (e.g., carbon nanotubes) have been studied in order to obtain structures with enhanced mechanical and/or electrical properties [7–12]. Among other conductive polymers, much attention has been drawn to polyaniline (PANI) [13]. Mechanical, electrical and functional properties of PANI films and fibers, either of the bare polymer or of PANI-based nanocomposites, have been investigated [4–6,9–11,14–24]. Nevertheless, when dealing with nanocomposite PANI fibers, as well as with other nanocomposite polymeric structures, such properties have to be characterized through different length scales, from those of the whole structures – generally meso- or micro-scales – down to those of the nanomaterials forming the composites. In particular, the investigation of samples properties at nanoscale requires techniques capable of probing the surface with nanometrical lateral resolution. Due to its capability of probing the sample using a tip with radius of few nanometers placed in close vicinity of the sample surface, atomic force microscopy (AFM) [25] has been proposed as a tool to develop several techniques for mapping different physical properties simultaneously to the morphological reconstruction with nanometrical lateral resolution. More specifically, as a consequence of the deflection of the cantilever, the AFM tip exerts a force on the sample surface. The latter is

* Corresponding author. Tel.: +39 06 49766591; fax: +39 06 49766932.
E-mail address: daniele.passeri@uniroma1.it (D. Passeri).

0014-3057/$ - see front matter © 2013 Elsevier Ltd. All rights reserved.
http://dx.doi.org/10.1016/j.eurpolymj.2013.02.003

locally deformed, which allows one to evaluate the mechanical properties of the volume of the sample immediately under the tip. In addition, using tips and cantilevers coated with conductive ultra-thin films and conductive substrates, a voltage can be applied between the tip and the sample and the corresponding electric current can be recorded. This allows one to characterize the electrical properties of the sample.

In this work, we report the morphological, electrical and mechanical characterization of nanocomposite fibers obtained by chemical polymerization of PANI in presence of detonation nanodiamond (DND) particles. Such characterizations have been performed using different AFM-based techniques. Morphological characterization has been carried out in standard AFM semi-contact mode. Electrical characterization has been performed taking advantage of AFM-based experimental setup modified for the purpose. Finally, mechanical characterization of the PANI/DND fibers has been performed synergically using two different techniques, namely torsional harmonic AFM (TH-AFM) [26,27] and contact resonance AFM (CR-AFM) [28,29], which are a tapping mode and contact mode based technique, respectively.

2. Samples description

PANI/DND fibers were prepared by precipitation polymerization of aniline monomer in presence of DND particles in aqueous solution. An anionic surfactant, i.e., sodium dodecyl sulfate (SDS), was used to facilitate the DND dispersion in the reaction environment. Ammonium persulfate was used as radical initiator following the reaction protocol described elsewhere [30]. For AFM characterizations, PANI/DND fibers networks were collected on monocrystalline Si substrates. A complete characterization of the obtained PANI/DND fibers has been performed using optical microscopy, both transmission and scanning electron microscopy (TEM and SEM, respectively), Raman spectroscopy, reflection high energy electron diffraction (RHEED), X-ray diffraction (XRD), and thermo gravimetric analysis (TGA), which can be found elsewhere [30]. The polymerization resulted in the formation of a tightly woven network of nanocomposite fibers. Structural characterization suggested that DND particles, which behave as "seeds" for the growth of PANI in form of fibers instead of films, are included in the inner of the fibers. Moreover, RHEED and XRD characterizations suggest that both DND particles and PANI chains have preferred orientations, the last ones being orderly arranged in the direction perpendicular to the fiber axis [30].

3. Techniques

Morphological characterization of PANI/DND fibers has been performed in AFM semi-contact mode using our AFM apparatus (Solver, NT-MDT, Russia) equipped with Si cantilevers (NSG10, NT-MDT, Russia).

3.1. Electrical characterization

To verify the conductivity of PANI/DND fibers, their electrical characterization has been performed equipping the aforementioned AFM apparatus with contact mode Si cantilevers coated with conductive Pt ultra-thin films (CSG10/Pt, NT-MDT, Russia). The experimental setup is inspired to that for scanning spreading resistance microscopy [31–33]. In the latter, a dc voltage is applied between the (conductive) tip and the (conductive) sample substrate and the dc electric current is detected that flows through the sample in the direction normal to its surface. Conversely, in our experimental setup an electrode was realized at one end of the fiber network [30]. Thus, applying a dc voltage between the tip and the electrode, the dc electric current I_{t-e} flowing from the tip to the electrode is detected. Therefore, when the tip is in contact with the fiber surface, I_{t-e} is the current flowing along the main axis of the fiber. Finally, maps of I_{t-e} can be acquired simultaneously to the morphological reconstruction, which reflect the conductivity of the nanocomposite fiber [30].

3.2. Mechanical characterization

For TH-AFM, the AFM apparatus (Dimension Icon, Bruker Inc.) was equipped with a *T*-shaped cantilever with out-of-axis tip (HMX10, Bruker Inc.), with first free flexural resonance in air $f_1^0 = 54.2$ kHz and first free torsional resonance in air $t_1^0 = 964$ kHz. The sample is imaged in standard tapping mode at f_1^0. The surface of compliant samples is thus periodically indented by the tip with period $T = 1/f_1^0$. Therefore, during each cycle a complete approaching (loading) and retracting (unloading) force–distance curve could be obtained. The periodicity of the signal would suggest collecting the spectrum and analyzing it by inverse Fourier transform, which nevertheless is prevented by the presence of the higher flexural modes of the cantilever that distort the spectrum. To circumvent such limitation, the cantilever torsional signal can be used [26,27]. Indeed, the out-of-axis tip excites the periodic torsion (with period *T*) of the cantilever that is enhanced by its shape [26,27]. The torsional signal can be reconstructed by inverse Fourier transform of its spectrum, as it contains several harmonics of f_1^0 unaltered by the torsional resonance, t_1^0 being about 20 times higher that f_1^0. Therefore, after proper analysis, force–distance and thus force–indentation curves are obtained from the torsional signal [26,27]. By fitting the initial portion of the unloading force–distance curve using the Derjaguin–Muller–Toporov (DTM) model, the sample indentation modulus $M = E/(1 - \nu^2)$ can be evaluated, where E and ν are the Young's modulus and the Poisson ratio of the sample, respectively. In addition, other mechanical parameters can be deduced that depend on both the tip/cantilever and the sample, like the maximum force exerted on the sample (F_{max}), the tip–sample adhesion (F_{adh}) and the energy dissipated during one loading–unloading cycle (E_{diss}). Taking advantage of high speed data acquisition, such parameters can be evaluated at each point of the scanned area and thus mapped simultaneously to the morphological reconstruction. Quantitative mapping of the sample mechanical properties

has been performed after calibration of the technique using the procedure indicated by the manufacturer and adopting a blend of polystyrene (PS) and low density polyethylene (LDPE) with known mechanical properties (PS/LDPE by Bruker Inc.) as the reference sample. In particular, the PS/LDPE sample is characterized by well distinguishable areas associated to the PS and LDPE polymeric phase, respectively. Thus, the tip is calibrated assuming M_{PS} = 1.6 GPa for the PS phase. Such a value is that reported by the manufacturer and was not verified by independent techniques. The LDPE phase is used as a control reference material, its indentation modulus being given by the manufacturer as high as M_{LDPE} = 100 MPa. Really, monitoring M_{LDPE} on several measurements performed in our laboratory over a one year's time, we obtained M_{LDPE} = 100 ± 24 - MPa. No trends in the measured M_{LDPE} were observed so that fluctuations in its value should be attributed solely to random errors and not to systematic factors such as aging of the sample, although according to the producer variation of PS/LDPE mechanical properties over the time is 'only approximately known'. Assuming the same uncertainty for M_{PS} and M_{LDPE}, it can be evaluated as high as 12%. In addition, we should also note that the indentation modulus measured on the PS phase randomly varies, mainly due to fluctuations in the tip–sample contact area produced by the surface roughness. Nevertheless, due to the high number of sampled points (generally 256×256 points over a few square microns), values of M_{PS} are generally normally distributed around a very well defined peak value with a standard deviation that, for the measurements reported in this work, is as high as 14%.

For CR-AFM, the AFM apparatus (Solver, NT-MDT, Russia) has been equipped with Si cantilevers (CSG10, NT-MDT, Russia). The back of the sample is coupled to a piezoelectric transducer that excites out-of-plane vibration of the sample surface at ultrasonic frequencies [34,35]. This produces the modulation of the indentation depth and the presence of an oscillating component in the cantilever deflection signal. Cantilever flexural resonances depend on the tip–sample contact mechanics. In particular, the cantilever can be modeled as a uniform beam with rectangular cross section parallel to the sample surface, as sketched in Fig. 1. The contact between the tip and a viscoelastic sample can be modeled as the parallel between a spring (namely, the normalized contact stiffness α) and a dashpot (namely, the normalized contact damping coefficient β) [28]. These two parameters determine the frequency response of the system and the spectrum of the cantilever deflection signal can be acquired and analyzed to evaluate the viscoelastic properties of the sample. α and β can be deduced from the values of the cantilever contact resonance frequencies f_n's and the corresponding Q-factor Q_n's [28,29]. The mechanical response of viscoelastic materials can be described by the complex modulus $M_s = M'_s + iM''_s$, where M' and M'' are the sample storage and loss modulus, respectively. After determining α and β for the investigated sample (α_s and β_s) and a reference (α_{ref} and β_{ref}), M'_s and M''_s can be evaluated as $M'_s = M'_{ref}(\alpha_s/\alpha_{ref})^{3/2}$ and $M''_s = M''_{ref}(f_s\beta_s/f_{ref}\beta_{ref})^{3/2}$, where: f_s and f_{ref} are the contact frequencies measured on the sample and the reference, respectively; M'_{ref} and M''_{ref} are the storage and loss moduli of the reference sample, respectively; finally, the exponent 3/2 derives from assuming a spherical apex of the AFM tip [28,29]. In this work, quantitative mechanical measurements have been obtained after calibration using a LDPE and a polycarbonate (PC) thick samples (supplied by Goodfellow) as two references, according to the procedure described by Stan and Price [36]. In particular, we have already reported the indentation modulus values of such samples measured by standard nanoindentation, which we used for the calibration of AFM-based nanoindentation [37,38]. In addition, we measured the indentation modulus of such samples also by TH-AFM obtaining M_{LDPE} = 330 ± 97 MPa and M_{PC} = 1.2 ± 0.2 GPa. While the value for LDPE is coherent with both standard and AFM-based nanoindentation ones, that for PC is significantly lower than those retrieved by nanoindentation techniques. Really, the comparison of the results retrieved using the three techniques reveals that the measured M_{LDPE}/M_{PC} ratio increases with the decreasing of the penetration depth [39]. As the penetration depth typical of CR-AFM is more similar to that of TH-AFM than those of standard or AFM-based nanoindentations, the values of M_{LDPE} and M_{PC} measured by TH-AFM have been used as the reference values for M' in CR-AFM. Conversely, no calibration values were available for M'' and thus the measured values of M'' will be given as the ratio with those retrieved on one of the references.

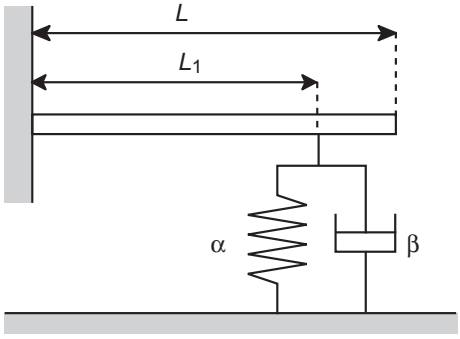

Fig. 1. Sketch of the model assumed for the analysis of CR-AFM results. The cantilever is supposed to be parallel to the sample surface, while the tip–sample contact is modeled as the parallel between the normalized contact stiffness α and the normalized damping coefficient β.

4. Results and discussion

4.1. Morphological characterization

PANI/DND sample consists of a dense network of fibers and ribbons. Fig. 2 reports an optical image of the sample, acquired in dark field observation mode, showing typical fibers and ribbons with width of a few microns and length of some hundreds of microns. A more detailed characterization of the morphology of PANI/DND fibers has been carried out by AFM. Fig. 3a shows that fibers and ribbons observed by optical microscopy actually consist of bundles of fibrils, either parallel or twisted. A detail of a fiber

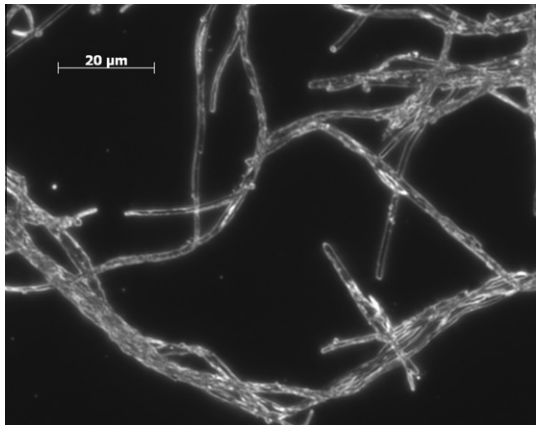

Fig. 2. Optical image of the PANI/DND sample, acquired in dark field observation mode.

(Fig. 3b) and one of its cross sections (Fig. 3b) reveal that the fibrils have a roughly circular section with diameter of a few hundreds of nanometers. These are bundled in ribbons with height approximately equal to the fibril diameter and width of a few microns, which is bound to be induced by the presence of the substrate.

4.2. Electrical characterization

Fig. 4 reports the topographical image of PANI/DND fibers with superimposed two electric current maps (the two cyan insets). I_{t-e} has been acquired by applying a tip-electrode voltage V_{t-e} = +2 V (upper inset) or V_{t-e} = −2 V (lower inset): as expected, the sign of I_{t-e} reverses correspondingly. A rough estimation of the electrical resistance R_f of PANI/DND fibers can be carried out considering that for V_{t-e} = +2 V the measured current is approximately I_{t-e} = 20 nA and thus R_f = 100 MΩ. To evaluate the electrical conductivity σ of the PANI/DND nanocomposite from the measurement of R_f, we simulated the electric current flow into the fiber when a dc voltage is applied between the realized electrode and the AFM tip, using a commercial finite element analysis (FEA) software (Comsol Multiphysics). Fig. 5a and b show the three dimensional and the side view, respectively, of the streamline of the electric current density along the fiber. The latter is approximated as a beam with square cross section (1 μm × 1 μm) and $\sigma = 10^3$ S m^{-1}. The electrode ($\sigma = 10^7$ S m^{-1}) is placed in correspondence of the first section of the fiber. The second electrode ($\sigma = 10^7$ S m^{-1}), constituted by the conductive AFM tip, is a square with side of 10 nm placed on the upper surface of the fiber. Fig. 5c and d report the electric current density map in correspondence of the sections marked with 1 and 2 in Fig. 5b, respectively. Very near the tip (Fig. 5c) the current density is not uniform, the difference between its maximum and minimum values being the 95% of the maximum value. Nevertheless, at a distance from the tip larger than about 1 μm, the current density becomes almost uniform along the fiber and constant in the cross section. As an example, in Fig. 5d the difference between its maximum and minimum values is only the

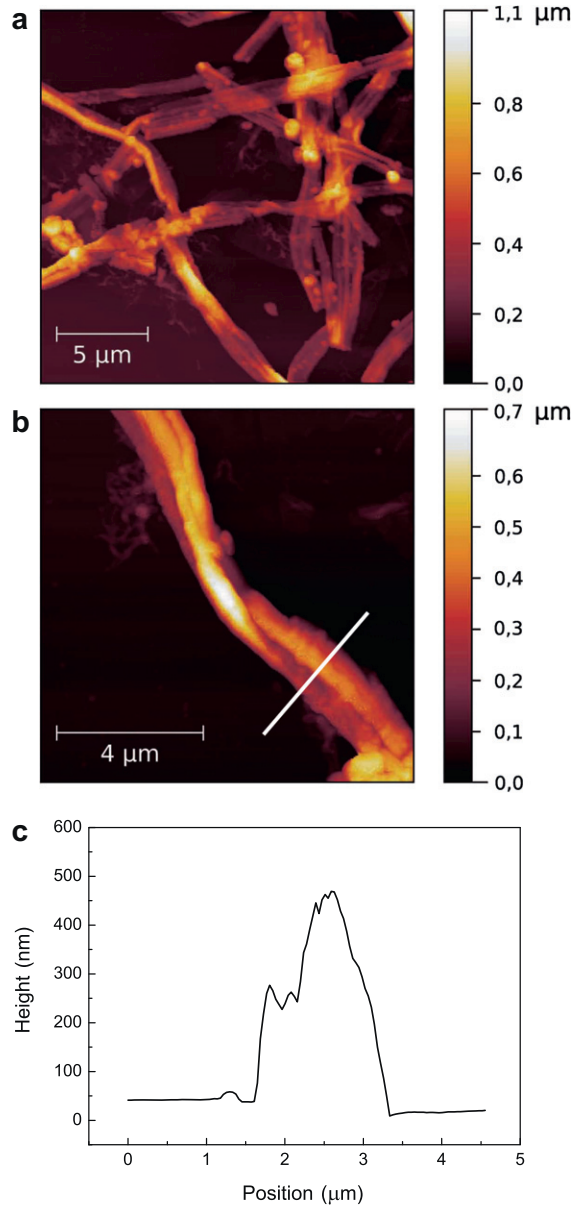

Fig. 3. (a) AFM image of PANI/DND sample, showing that fibers and ribbons forming the network consist of bundles of fibrils. (b) Detail of a PANI/DND fiber and (c) cross section profile in correspondence of the white segment in (b).

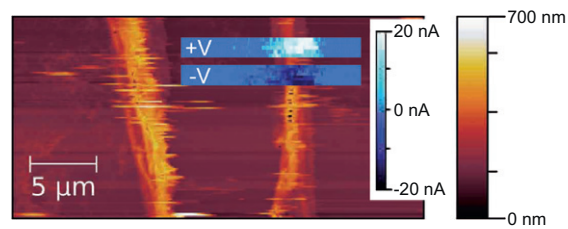

Fig. 4. Image of two PANI/DND fibers with superimposed the corresponding electrical characterization. In the insets, the I_{t-e} maps are reported obtained applying V_{t-e} = +2 V (upper inset) or V_{t-e} = −2 V (lower inset).

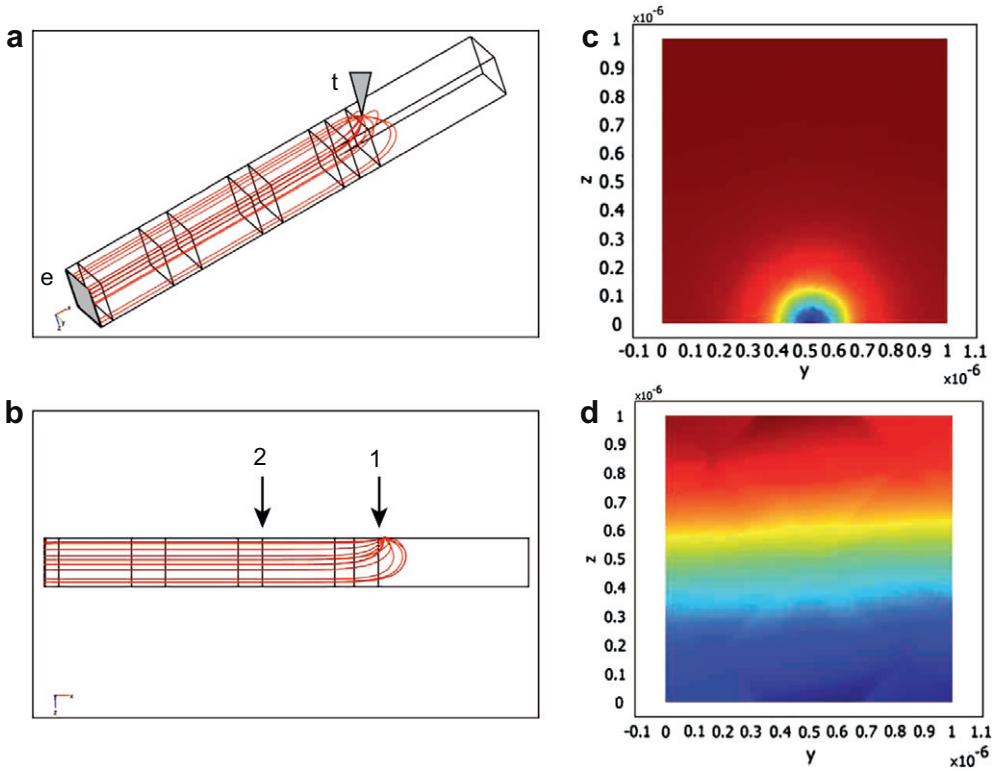

Fig. 5. Three dimensional (a) and side view (b) of the simulated fiber: a direct voltage is applied between the electrode (e) and the AFM tip (t) and the streamline of the electric current density is shown. (c) Current density map in correspondence of the section marked with 1 in (b) where the full range of the color bar is the 95% of the current density maximum value. (d) Current density map in correspondence of the section marked with 2 in (b) where the full range of the color bar is the 0.0002% of the current density maximum value.

0.0002% of the maximum value. As suggested by the FEA simulation, the fiber can be modeled as cylindric conductor with uniform section S, length l and overall resistance R. As a consequence, σ of the PANI/DND nanocomposite can be estimated as $\sigma = l(RS)^{-1}$ thus giving values ranging from tens to hundreds of S m^{-1}, the high variability being related to the uncertainty in the fiber length and section. Being in the range of those reported for PANI fibers [16], such values suggest that the presence of DND particles does not affect the conductivity of the nanocomposite fibers. Note that in absence of DND and maintained all the other experimental conditions fixed, aniline monomer polymerization did not result in fibers formation, preventing the definitive assessment of DND effect on the electrical conductivity of the nanocomposite.

4.3. Mechanical characterization

Fig. 6a shows the morphology of a typical PANI/DND fiber while Fig. 6b reports the corresponding quantitative map of indentation modulus obtained by TH-AFM. Fig. 6c shows the statistics of the indentation modulus values of the PANI/DND fiber retrieved by 6b. Note that the values of the indentation modulus of the bright regions in Fig. 6b corresponding to the stiff substrate are fictitious, exceeding the calibration range. Apparently, indentation modulus of PANI/DND fiber is found as high as $M_f = 1.0 \pm 0.5$ GPa. Really, the histogram in Fig. 6c can be interpreted as the convolution of two Gaussian distributions centered in 0.5 GPa (with standard deviation 0.24 GPa) and 1.2 GPa (with standard deviation 0.4 GPa), respectively. The former value, associated to the step slopes of the fiber, is due to the reduction of the tip–sample contact area and therefore should not be considered as real. Thus, the mean value of the indentation modulus of the PANI/DND fiber is 1.2 GPa. Ten analogous measurements have been performed on different fibers or different locations of the same fibers and fiber indentation modulus values have been obtained in the range 1.1–1.8 GPa. Such values are significatively lower than those we measured on pure PANI thin films by AFM nanoindentation [40], although they are in the range of those reported in literature [9,10,15,16]. Really, due to their geometry, elastic modulus of PANI/DND fibers is expected to be anisotropic. Literature values of elastic modulus of PANI fibers are generally measured by tensile tests and thus refer to the elastic modulus in the direction of the main axis of the fiber. Actually, indentation modulus values reported in this work are measured perpendicularly to the fibers main axis. Moreover, one should consider that TH-AFM indentation depth into the sample is limited to few nanometers. Thus, such a technique probes a volume of the sample very near to the surface, where deviations of the mechanical properties from those of the bulk material can occur [39]. Since

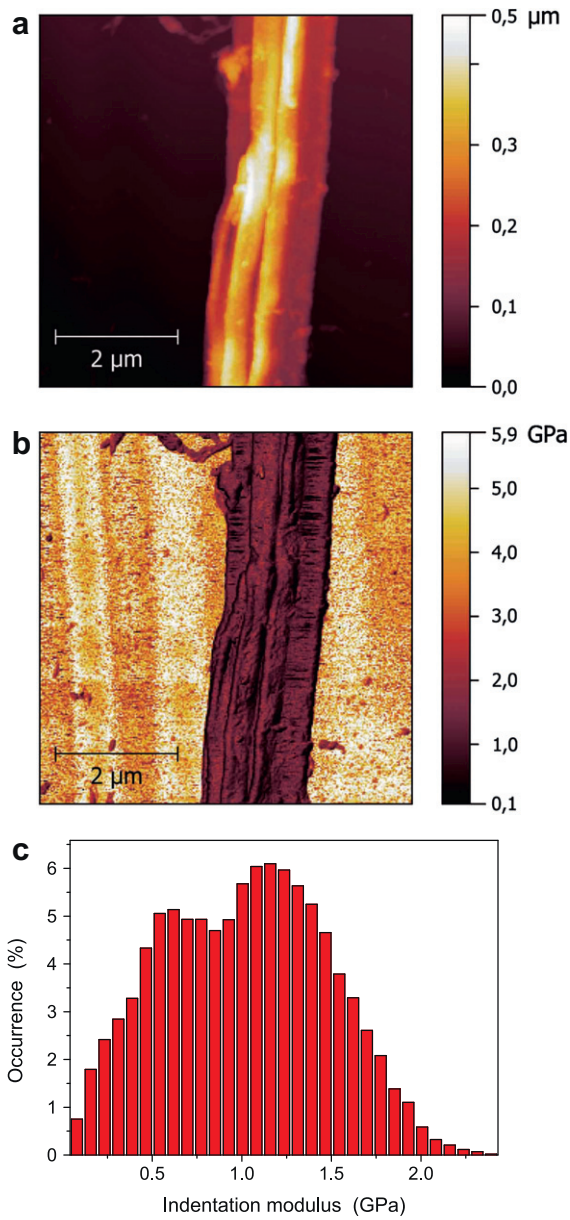

Fig. 6. Morphology (a) and corresponding quantitative indentation modulus map (b) of a typical PANI/DND fiber, obtained by TH-AFM. (c) Statistics of the indentation modulus values reported in (b) in correspondence of the PANI/DND fiber.

DND indentation modulus is about three orders of magnitude higher than that of PANI, it should increase the elastic modulus of the nanocomposite. So, the previous consideration suggests that DND particles are located in the inner of the fiber well below its surface, in agreement with the results of the structural characterization [30].

To confirm TH-AFM results, we performed CR-AFM imaging of the PANI/DND nanocomposite fibers. Fig. 7a and b show the map of the third contact resonance frequency and the corresponding *Q*-factor, respectively, acquired on an isolated PANI/DND fiber. As expected, values of both f_3 and Q_3 in correspondence of the fiber are lower than those in correspondence of the Si substrate. Fig. 7c and d report the statistics of f_3 and Q_3 in correspondence of the fiber, respectively. From the mean values of f_3 and Q_3, those of α and β are obtained for the PANI/DND fiber. Using the values of α measured on the LDPE and PC reference samples, $M'_f = 2.6$ GPa is obtained for the fiber. Being CR-AFM far more time consuming than TH-AFM (which increases the required tip–sample contact time and consequently the possibility of modification of the tip shape during a single image acquisition) and considering the high variability of the measured values of *f* and *Q* on the same fiber, only one fiber has been characterized by such a technique. Note that TH-AFM and CR-AFM are performed on different fibers, and thus a certain variability in the elastic modulus is expected. Also, the statistics reported in Fig. 6c and in Fig. 7c and d reveal a significant variability in the elastic modulus values measured on the same fiber, due to both real inhomogeneity in the mechanical properties and apparent variations due to artifacts induced by changes in the sample morphology that are reflected into variation in the tip–sample contact radius [39]. In addition, it should be allowed for possible imperfections of the surface of the LDPE and PC references used for CR-AFM that would produce a not homogeneity of their surface mechanical properties at macro- or meso-scale, which would affect the uncertainty in the reference values for calibration. It should be noted that the comparison between data obtained with the two methods is possible as the indentation modulus of the reference samples used for calibration of CR-AFM has been previously determined using TH-AFM. Nevertheless, the uncertainty in the indentation modulus of the PANI/DND fiber determined using CR-AFM is increased by that in the values of the indentation moduli of the LDPE and PC samples used as references for CR-AFM and measured by TH-AFM. As a final remark, due to the calibration procedure we followed, all the values of indentation modulus can be considered as obtained 'for comparison' with the modulus of the PS polymeric phase of the PS/LDPE reference sample used for TH-AFM. Nevertheless, the higher value of indentation modulus measured by CR-AFM with respect to that by TH-AFM can be rationalized considering that the static load continuously applied by CR-AFM was 3–4 times higher than the peak load applied by TH-AFM. Thus, the latter technique probes a smaller volume of sample under its surface virtually unaffected by the substrate properties. Conversely, the former technique is more affected by the mechanical properties of the inner of the fiber and of the substrate. Therefore, the higher modulus retrieved by CR-AFM is the effect of the DND particles in the inner of the fiber and/or of the Si substrate. Finally, for the PANI/DND fiber loss modulus, we obtained $M''_f/M''_{PC} = 2.5$. For comparison, for the two references we obtained $M''_{LDPE}/M''_{PC} = 5.4$.

5. Conclusion

In conclusion, we described the morphological, electrical and mechanical characterizations of PANI/DND nanocomposite fibers performed by AFM techniques.

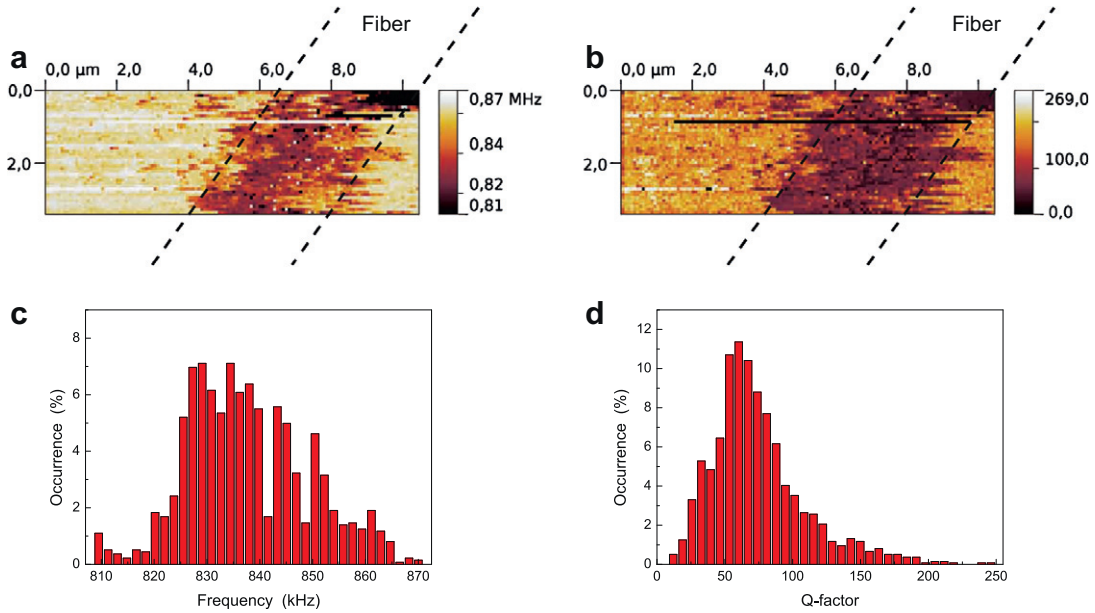

Fig. 7. Map of the cantilever third mode contact resonance frequency (a) and *Q*-factor (b) of a typical PANI/DND fiber, obtained by CR-AFM. Statistics of the values of contact resonance frequency (c) and *Q*-factor (d) in correspondence of the fiber.

Morphological study by standard AFM supplied information about the fibrillar structure of PANI/DND fibers and ribbons. Electrical characterization by an AFM based technique we specifically developed for the purpose revealed that PANI/DND fibers and ribbons are conductive and allowed us to roughly estimate their conductivity. Mechanical characterization was carried out by two different techniques, one based on semi-contact and one based on contact AFM operation mode. The former was sensitive to the near surface mechanical properties of the fibers, while the latter was affected also by the mechanical properties of the inner of the fibers, where DND particles are located, and of the substrate.

References

[1] Daoud WA, Xin JH, Szeto YS. Polyethylenedioxythiophene coatings for humidity, temperature and strain sensing polyamide fibers. Sens Actuat B 2005;109:329–33.
[2] Jang J, Chang M, Yoon H. Chemical sensors based on highly conductive poly 3,4-ethylenedioxythiophene nanorods. Adv Mater 2005;17:1616–20.
[3] Abidian MR, Kim DH, Martin DC. Conducting-polymer nanotubes for controlled drug release. Adv Mater 2006;18:405–9.
[4] Mazzoldi A, Degl'Innocenti C, Michelucci M, De Rossi D. Actuative properties of polyaniline fibers under electrochemical stimulation. Mater Sci Eng C Biomim 1998;6:65–72.
[5] Smela E, Lu W, Mattes BR. Polyaniline actuators. Part 1. PANI(AMPS) in HCl. Synth Met 2005;151:25–42.
[6] Smela E, Mattes BR. Polyaniline actuators. Part 2. PANI(AMPS) in methanesulfonic acid. Synth Met 2005;151:43–8.
[7] Selmi A, Friebel C, Doghri I, Hassis H. Prediction of the elastic properties of single walled carbon nanotube reinforced polymers: a comparative study of several micromechanical models. Compos Sci Technol 2007;67:2071–84.
[8] Ishiyama C, Higo Y. Elastic modulus of single-walled carbon nanotube/poly(methyl methacrylate) nanocomposites. J Polym Sci B Polym Phys 2004;42:2286–93.
[9] Mottaghitalab V, Spinks GM, Wallace GG. The influence of carbon nanotubes on mechanical and electrical properties of polyaniline fibers. Synth Met 2005;152:77–80.
[10] Gajendran P, Saraswathi R. Polyaniline–carbon nanotube composites. Pure Appl Chem 2008;11:2377–95.
[11] Soundararajah QY, Karunaratne BSB, Rajapakse RMG. Montmorillonite polyaniline nanocomposites: (preparation), characterization and investigation of mechanical properties. Mater Chem Phys 2009;113:850–5.
[12] Tamburri E, Orlanducci S, Terranova ML, Valentini F, Palleschi G, Curulli A, et al. Modulation of the electrical properties in single-walled carbon nanotube/conducting polymer composites. Carbon 2005;43:1213–21.
[13] Long YZ, Li MM, Gu C, Wan M, Duvail JL, Liu Z, et al. physical properties and applications of conducting polymer nanotubes and nanofibers. Prog Polym Sci 2011;36:1415–42.
[14] Pomfret SJ, Adams PN, Comfort NP, Monkman AP. Inherently electrically conductive fibers wet spun from a sulfonic acid-doped polyaniline solution. Adv Mater 1998;10:1351–3.
[15] Singh U, Prakash V, Abramson AR, Chen W, Qu L, Dai L. Mechanical characterization device for *in situ* measurement of nanomechanical properties of micro/nanostructures. Appl Phys Lett 2006;89:073103.
[16] Wang HL, Romero RJ, Mattes BR, Zhu Y, Winokur MJ. Effect of processing conditions on the properties of high molecular weight conductive polyaniline fiber. J Polym Sci B Polym Phys 2000;38:194–204.
[17] Wang HL, Gao J, Sansiñena JM, McCarthy P. Fabrication and characterization of polyaniline monolithic actuators based on a novel configuration: integrally skinned asymmetric membrane. Chem Mater 2002;14:2546–52.
[18] Herrasti P, Ocón P, Ibáñez A, Fatás E. Electroactive polymer films for stainless steel corrosion protection. J Appl Electrochem 2003;33:533–40.
[19] Deore BA, Yu I, Aguiar PM, Recksiedler C, Kroeker S, Freund MS, et al. self-doped polyaniline exhibiting unprecedented hardness. Chem Mater 2005;17:3803–5.
[20] Kang ET, Ma ZH, Tan KL, Tretinnikov ON, Uyama Y, Ikada Y. Surface hardness of pristine and modified polyaniline films. Langmuir 1999;15:5389–95.
[21] Lesueur D, Colin X, Camino G, Albérola ND. Dynamic mechanical behaviour and thermal degradation of undoped polyaniline. Polym Bull 1997;39:755–60.
[22] Tamburri E, Orlanducci S, Guglielmotti V, Reina G, Rossi M, Terranova ML. Engineering detonation nanodiamond e polyaniline composites by electrochemical routes: structural features and functional characterizations. Polymer 2011;52:5001–8.
[23] Xiong S, Wang Q, Chen Y. Study on electrical conductivity of single polyaniline microtube. Mater Lett 2012;45:4238–46.

[24] Zhang Y, Rutledge GC. Electrical conductivity of electrospun polyaniline and polyaniline-blend fibers and mats. Macromolecules 2012;45:4238–46.
[25] Binnig G, Quate CF, Gerber C. Atomic force microscope. Phys Rev Lett 1986;56:930–3.
[26] Sahin O, Magonov S, Su C, Quate CF, Solgaard O. An atomic force microscope tip designed to measure time-varying nanomechanical forces. Nat Nanotechnol 2007;2:507–14.
[27] Sahin O, Erina N. High-resolution and large dynamic range nanomechanical mapping in tapping-mode atomic force microscopy. Nanotechnology 2008;19:445717.
[28] Yuya PA, Hurley DC, Turner JA. Contact-resonance atomic force microscopy for viscoelasticity. J Appl Phys 2008;104:074916.
[29] Yuya PA, Hurley DC, Turner JA. Relationship between Q-factor and sample damping for contact resonance atomic force microscope measurement of viscoelastic properties. J Appl Phys 2011;109:113528.
[30] Tamburri E, Guglielmotti V, Orlanducci S, Terranova ML, Sordi D, Passeri D, et al. Nanodiamond-mediated crystallization in fibers of PANI nanocomposites produced by template-free polymerization: conductive and thermal properties of the fibrillar networks. Polymer 2012;53:4045–53.
[31] De Wolf P, Clarysse T, Vandervorst W, Hellemans L, Niedermann P, Hänni W. Cross-sectional nano-spreading resistance profiling. J Vac Sci Technol B 1998;16:355–61.
[32] De Wolf P, Geva M, Hantschel T, Vandervorst W, Bylsma RB. Two-dimensional carrier profiling of InP structures using scanning spreading resistance microscopy. Appl Phys Lett 1998;73:2155–7.
[33] Oliver RA. Advances in AFM for the electrical characterization of semiconductors. Rep Prog Phys 2008;71:076501.
[34] Passeri D, Bettucci A, Germano M, Rossi M, Alippi A, Sessa V, et al. Local indentation modulus characterization of diamond-like carbon films by atomic force acoustic microscopy two contact resonance frequencies imaging technique. Appl Phys Lett 2006;88:121910.
[35] Passeri D, Bettucci A, Rossi M. Acoustic and atomic force microscopy for the mechanical characterization of thin films. Anal Bioanal Chem 2010;396:2769–83.
[36] Stan G, Price W. Quantitative measurements of indentation moduli by atomic force acoustic microscopy using a dual reference method. Rev Sci Instrum 2006;77:103707.
[37] Passeri D, Bettucci A, Biagioni A, Rossi M, Alippi A, Lucci M, et al. Quantitative measurement of indentation hardness and modulus of compliant materials by atomic force microscopy. Rev Sci Instrum 2008;79:066105.
[38] Passeri D, Bettucci A, Biagioni A, Rossi M, Alippi A, Tamburri E, et al. Indentation modulus and hardness of viscoelastic thin films by atomic force microscopy: a case study. Ultramicroscopy 2009;109:1417–27.
[39] Passeri D, Rossi M, Tamburri E, Terranova ML. Mechanical characterization of polymeric thin films by atomic force microscopy based techniques. Anal Bioanal Chem 2013;405:1463–78.
[40] Passeri D, Alippi A, Bettucci A, Rossi M, Alippi A, Tamburri E, et al. Indentation modulus and hardness of polyaniline thin films by atomic force microscopy. Synth Met 2011;161:7–12.